Nano Research
2022, 15(10): 9639–9646

ISSN 1998-0124 CN 11-5974/O4
https://doi.org/10.1007/s12274-022-4570-5

Research Article

Yb- and Er concentration dependence of the upconversion luminescence of highly doped $NaYF_4$:Yb,Er/$NaYF_4$:Lu core/shell nanocrystals prepared by a water-free synthesis

Christian Würth[1], Bettina Grauel[1], Monika Pons[1], Florian Frenzel[1], Philipp Rissiek[2], Kerstin Rücker[1], Markus Haase[1] (✉), and Ute Resch-Genger[1] (✉)

[1] *Federal Institute for Materials Research and Testing (BAM), Division Biophotonics, Richard-Willstaetter-Str. 11, 12489 Berlin, Germany*
[2] *Institut für Chemie Neuer Materialien, Fachbereich Biologie/Chemie, Universität Osnabrück, Barbarastraße 7, 49076 Osnabrück, Germany*

Received: 20 April 2022 / **Revised:** 10 May 2022 / **Accepted:** 21 May 2022

ABSTRACT

High sensitizer and activator concentrations have been increasingly examined to improve the performance of multi-color emissive upconversion (UC) nanocrystals (UCNC) like $NaYF_4$:Yb,Er and first strategies were reported to reduce concentration quenching in highly doped UCNC. UC luminescence (UCL) is, however, controlled not only by dopant concentration, yet by an interplay of different parameters including size, crystal and shell quality, and excitation power density (*P*). Thus, identifying optimum dopant concentrations requires systematic studies of UCNC designed to minimize additional quenching pathways and quantitative spectroscopy. Here, we quantify the dopant concentration dependence of the UCL quantum yield (Φ_{UC}) of solid $NaYF_4$:Yb,Er/$NaYF_4$:Lu upconversion core/shell nanocrystals of varying Yb^{3+} and Er^{3+} concentrations (Yb^{3+} series: 20%–98% Yb^{3+}; 2% Er^{3+}; Er^{3+} series: 60% Yb^{3+}; 2%–40% Er^{3+}). To circumvent other luminescence quenching processes, an elaborate synthesis yielding OH-free UCNC with record Φ_{UC} of ~ 9% and ~ 25 nm core particles with a thick surface shell were used. High Yb^{3+} concentrations barely reduce Φ_{UC} from ~ 9% (20% Yb^{3+}) to ~ 7% (98% Yb^{3+}) for an Er^{3+} concentration of 2%, thereby allowing to strongly increase the particle absorption cross section and UCNC brightness. Although an increased Er^{3+} concentration reduces Φ_{UC} from ~ 7 % (2% Er^{3+}) to 1% (40%) for 60% Yb^{3+}. Nevertheless, at very high *P* (> 1 MW/cm^2) used for microscopic studies, highly Er^{3+}-doped UCNC display a high brightness because of reduced saturation. These findings underline the importance of synthesis control and will pave the road to many fundamental studies of UC materials.

KEYWORDS

highly doped upconversion nanocrystals, core/shell nanoparticles, upconversion luminescence efficiency, $NaYF_4$:Yb, Er, concentration quenching

1 Introduction

Spectrally shifting multi-color emissive lanthanide-based upconversion (UC) nanocrystals (NC; UCNC), which can exhibit upconversion luminescence (UCL) and downshifted luminescence (DSL), hold great promise as reporters for bioimaging and biosensing, super-resolution microscopy, optogenetics, photodynamic and photothermal therapy, photocatalysis, anticounterfeiting and three-dimensional (3D) display technology [1–10]. UCNC typically consist of a transparent host matrix of high phonon energy doped such as $NaYF_4$ doped with the sensitizer/activator pairs Yb^{3+}/Er^{3+} or Yb^{3+}/Tm^{3+}. One challenge encountered for life and material sciences applications of UCNC is the relatively small absorption cross section of the particles. This quantity is determined by the concentration of the sensitizer Yb^{3+} that absorbs 978 nm excitation light and transfer this energy to the activator ions that subsequently emit photons of shorter energy in the ultraviolet (UV), visible (vis), and near infrared (NIR) in the case of UCL [1, 11]. The most straightforward strategy to enhance the absorption cross section of UCNC is to increase the Yb^{3+} concentration. In the absence of concentration quenching, this can automatically boost UCNC brightness, that determines the size of the measured luminescence signal from the material side and equals the product of the absorption cross section and the upconversion quantum yield (Φ_{UC}), a measure for UCL efficiency [3, 12]. Φ_{UC} is determined by the ratio of the number of emitted UCL photons, and the number of photons absorbed by the sensitizer. As UCL is a nonlinear multiphotonic process, Φ_{UC} depends on excitation power density (*P*). Thus, UCL and the signal size can be also tuned by *P* [13, 14] and high or ultrahigh *P* have been used to overcome UCL quenching processes, e.g., in microscopic studies [3, 15].

UCL efficiency can be diminished by surface defects, surface ligands, and solvent molecules containing high energy vibrators such as OH, and dopant ion concentrations [3, 15]. Moreover, it is well known from classical micrometer-sized phosphor materials that lanthanide doped luminescent materials display their highest quantum yields only within a limited concentration range of sensitizer and activator [11, 16]. For $NaYF_4$-based UC bulk materials utilizing Yb^{3+} as sensitizer and Er^{3+} or Tm^{3+} as activator, the optimum dopant concentrations are 18%–20% of Yb^{3+} and

Address correspondence to Markus Haase, markus.haase@uni-osnabrueck.de; Ute Resch-Genger, ute.resch@bam.de

2%–3% of Er^{3+} or 0.2%–0.5% of Tm^{3+}, respectively. Therefore, these concentrations have also been used in most studies on UCNC [13, 17–31]. A high Yb^{3+} concentration can decrease Φ_{UC} as a high number of sensitizers increases the mean energy migration length ("exciton diffusion radius") and therefore automatically enlarges the number of crystal defects and quenching sites within the particle and at the particle surface that are accessible via energy migration [18, 32, 33]. Particularly in core/shell nanocrystals of small size, all defects are within the energy migration length even at moderate sensitizer concentrations [34, 35]. In the case of the Er^{3+} activator, concentration quenching is mainly caused by cross relaxation [36, 37]. With the aim of improving the performance of UCNC, in recent years, higher sensitizer and activator concentrations have been increasingly examined and first strategies have been reported to reduce concentration quenching in highly doped UCNC [22, 29, 38, 39]. However, as UCL efficiency is not only affected by sensitizer and activator concentration, but also by an interplay of parameters such as crystal phase, crystal quality, UCNC size, number of defect sites formed in the crystal and at its surface during synthesis, thickness and quality of the surface shielding shell, and *P* [3], direct correlations between dopant ion concentration and UCL efficiency have not been derived.

To assess solely concentration quenching and identify optimum doping ion concentrations requires systematic studies with UCNC designed and prepared to prevent or at least minimize the impact of other UCL controlling parameters. In addition, the quantification of UCL concentration quenching calls for reliable absolute measurements of Φ_{UC} at different *P* commonly used for different applications with a properly calibrated integrating sphere setup [40]. The importance of quantifying concentration quenching for the field of UC nanomaterials encouraged us to explore the sensitizer and activator concentration dependence of Φ_{UC} at different *P* for highly doped solid 20–25 nm sized NaF_4:Yb,Er/$NaYF_4$:Lu core/shell UCNC with a thick and tight surface passivation shell prepared by a previously published elaborate water-free synthesis providing record Φ_{UC} values of 9 % for 45 nm core/shell $NaYF_4$:Yb,Er doped with 18%Yb^{3+} and 2% Er^{3+} [41]. These values closely approach those of high-quality microcrystals and are the highest Φ_{UC} values reported so far for UCNC [41]. For this study, we synthesized a series of UCNC from anhydrous rare earth acetates, where the Yb^{3+} concentration was varied from 20% to 98% and the Er^{3+} concentration was kept constant at 2% (Yb^{3+} concentration series), and UCNC with a high Yb^{3+} doping concentration of 60% and Er^{3+} concentrations varying from 2% to 40% (Er^{3+} concentration series). Quantitative spectroscopic studies with a calibrated and previously validated integrating sphere setup and solid UCNC revealed that for an Er^{3+} concentration of 2%, high Yb^{3+} concentrations only slightly reduce the record quantum yield of ~ 9 % (20% Yb^{3+}) to ~ 7% (98% Yb^{3+}). Although an increase in Er^{3+} concentration diminished Φ_{UC} from ~ 7% (2% Er^{3+}, 60% Yb^{3+}) to 1 % (40% Er^{3+}, 60% Yb^{3+}), at very high *P* (> 1 MW/cm^2) as utilized for microscopic studies, particles with a high Er^{3+} content nevertheless display a high brightness because of reduced saturation. These results will pave the road to the design of more fundamental photophysical studies of UCNC and to UCNC of increased brightness for different *P* regimes and applications in the life and material sciences without the need to utilize sophisticated tri- or multi-layer particle architectures [39] which can be easily prone to core/shell intermixing [42].

2 Experimental

2.1 Materials

Reagents. Oleic acid (purified, Fisher Scientific), 1-octadecene (technical grade 90%, Alfa Aesar), ammonium fluoride (min. 98.0%, Alfa Aesar), sodium oleate (82%, Sigma Aldrich), acetic acid (99.5%, Grüssing), acetic anhydride (Ph. Eur., VWR), yttrium oxide (99.9%, Intematix), ytterbium oxide and erbium oxide (99.9%, Chemos), lutetium oxide (99.99% Alfa Aesar). All materials were used as received. The anhydrous rare earth acetates were prepared as previously reported [41].

UCNC synthesis. We chose an elaborate synthetic method developed by us to prevent the intake of water and thus OH groups during synthesis which can provide $NaYF_4$:Yb,Er UCNC with record Φ_{UC} as earlier reported [41]. The high Φ_{UC} values approaching that of high-quality UC microcrystals underline the absence of UCL diminishing OH groups within the particles and a very small number of defects. The water-free syntheses of the α-Na_xYF_{3+x}:Yb,Er precursor particles for the β-$NaYF_4$:Yb,Er core particles, α-Na_xYF_{3+x}:Lu precursor particles for the β-$NaYF_4$:Lu shell, β-$NaYF_4$:Yb,Er core particles, and β-$NaYF_4$:Yb,Er/$NaYF_4$:Lu core/shell particles are detailed in the Electronic Supplementary Material (ESM).

2.2 Methods used for particle characterization

2.2.1 Structural characterization

Transmission electron microscopy (TEM) and X-ray powder diffraction (XRD) were used to determine the mean size, the size distribution [43], as well as the crystal phase and the phase purity of all particles [44, 45] respectively. The results are summarized in Figs. S1–S11 in the ESM. The lanthanide dopant ion concentrations were assumed to match the amounts of reagents used as a complete conversion of the lanthanide starting materials has been confirmed by many studies in both labs utilizing inductively coupled plasma optical emission spectrometry (ICP-OES) [46, 47].

2.2.2 Optical-spectroscopic characterization

2.2.2.1 P-dependent UCL spectra and upconversion quantum yields

The *P*-dependent UCL spectra and Φ_{UC} of the differently doped UCNC were determined absolutely with a calibrated, custom designed integrating sphere setup previously reported [40]. The setup included a very stable 8 W 976 nm laser diode as excitation light source and two filter wheels with neutral density filters of known transmittance, both in the excitation channel for controlled attenuation of *P* in small steps. Another filter wheel with edge, band pass, and neutral density filters is placed in the detection channel to avoid detector saturation. Detection of the transmitted and emitted photons was done with a silicon charge coupled device (CCD). The design and calibration of the setup, the beam profile characterization, and the measurement procedure were described in detail in a recent publication [40]. The reliability of these measurements was recently assessed in an international laboratory comparison on the determination of *P*-dependent Φ_{UC} of Yb,Tm-doped UCNC [48]. The calibration of the integration sphere setup and the calculation of Φ_{UC} from the measured UCL spectra and the number of absorbed photons are detailed in the ESM.

2.2.2.2 Time-resolved luminescence measurements

The luminescence decay kinetics were measured with an Edinburgh Instruments spectrofluorometer FLS-980 equipped with an electrically modulated 8 W 978 nm laser diode (40 μs long square pulse) and a red extended PMT (Hamamatsu R2658P). The decay curves were analyzed as previously reported [40]. The Yb^{3+} emission was always recorded at 1,000 nm.

2.2.2.3 Single particle studies

Single particle studies were performed on a custom-built confocal setup as described in Frenzel et al. [49]. Therefore, UCNC dispersions were diluted 1:10^5 with n-hexane and 3 μL of these diluted samples were pipetted onto a glass coverslip and dried at room temperature. From confocal scan images (80 μm × 80 μm) of the green and red UC luminescence under 980 nm excitation (LDH-D-F-980, PicoQuant, Germany), the single particles were detected by comparison of the relative intensities and choosing the least bright particles with similar brightness. For the confocal imaging a 100× oil-immersion objective with a numerical aperture of 1.4 (UPLSAPO100XO/1.4, Olympus) was used and for the detection a green (545 ± 12.5 nm; F49-546) and a red (655 ± 20 nm; F39-655) band-pass filter (AHF Analysetechnik AG, Germany) were placed in front of the APDs (PDM series, PicoQuant, Germany). The *P*-dependent UCL spectra were measured with a CCD camera iDus420 from ANDOR. Thereby, the laser intensity was varied in the cw mode concerning output power (30% to 100%) and by continuously pulsed repetition rates between 0.25 MHz and 80 MHz, covering a *P* range from 1×10^3 to 2×10^6 W/cm^2 [49].

3 Results and discussion

Essential for the quantification of the influence of the sensitizer and activator concentration on the Φ_{UC} of $NaYF_4$:Yb,Er UCNC are the minimization of other possible UCL quenching pathways by proper particle design and choice of sophisticated preparation methods [41] and the determination of the UCL characteristics, particularly the *P*-dependent key performance parameter Φ_{UC} with absolute and previously validated optical methods [40, 48]. Thereby, samples and instrument-related sources of uncertainty possibly contributing to these concentration studies can be strongly minimized.

3.1 Particle design, synthesis, and structural characterization

To maximize the UCL efficiency for high Yb^{3+} concentrations and thereby boost particle brightness, the number of defects in the core particle and at the core/shell interface must be as low as possible for all dopant concentrations to maximize the UCL efficiency for high Yb^{3+} concentrations. This is a prerequisite to assess solely the influence of high and very high Yb^{3+} doping concentrations. Of fundamental importance for this study were thus the choice of a suitable UCNC size and preparation method. In colloidal solution, $NaYF_4$ nanocrystals grow via Ostwald ripening and therefore exchange ions with the solution. This is a particular problem when the particle size is small because in this case the total surface area and the solubility of the particles are high, the latter due to the Gibbs-Thompson effect [50–52]. Moreover, ion exchange reactions can take place at the particles' surface when additional ions exist in solution, e.g., during shell formation. Ions, released into the solution from the core particles, can be incorporated into the shell, resulting in partial intermixing of core and shell materials [42, 53]. This is a problem particularly for core/shell particles with a thin shell and a highly doped core, because in this case, the concentration of dopant ions in the shell can be so high that energy migration through the shell is not sufficiently blocked. Highly doped core particles of small size are therefore the most difficult systems to shield with a thin shell. Ineffective shielding, however, results in additional surface quenching and must be therefore avoided for a study focusing on the effect of high dopant concentrations on Φ_{UC} of $NaYF_4$:Yb,Er nanocrystals.

Therefore, for our systematic study on sensitizer and activator concentration quenching in highly doped $NaYF_4$:Yb,Er UCNC with minimum distorting contributions from other common quenching pathways, we took three measures from the sample side. First, we restricted our study to comparatively large UCNC with core sizes in the range of 20–25 nm and a thick surface shell of 7–10 nm. In our previous study on the Φ_{UC} of $NaYF_4$:Yb,Er/$NaYF_4$ core/shell particles with the standard concentrations of Yb^{3+} and Er^{3+} of 18% and 2%, respectively, particles of this size and shell thickness already approached the Φ_{UC} value of the bulk material [41]. Second, we utilized an elaborate synthetic method developed by us that prevents the intake of water and thus OH groups [33] and provided $NaYF_4$:Yb,Er UCNC with the highest Φ_{UC} values reported so far for such relatively small particles [41]. Therefore, anhydrous rare earth acetates were used as precursors and the oleic acid/octadecene solvent was dried at high temperature for the preparation of UCNC cores and the subsequent shelling procedures. Third, the $NaYF_4$ shells were doped with Lu^{3+} to reduce the lattice mismatch between the highly doped particle core and the shell, employing Lu^{3+} concentrations in all cases that equaled the sum of the concentrations of both dopants in the core. Lu^{3+} has an ionic radius that is very similar to the radius of Yb^{3+} (and Er^{3+}) and is optically inert in the sense that it lacks 4f-4f transitions due to its completely filled 4f electron shell. Hence, it was to be expected that the presence of Lu^{3+} would not affect the Φ_{UC} of our UCNC.

3.1.1 *Structural characterization of the highly doped UCNC*

The subsequently performed syntheses of the UCNC of the Yb^{3+} and the Er^{3+} concentration series in oleic acid/octadecene yielded $NaYF_4$:Yb,Er core and $NaYF_4$:Yb,Er/$NaYF_4$:Lu core/shell UCNC with a narrow size distribution and an elongated shape for all concentrations of Yb^{3+}, Er^{3+}, and Lu^{3+} as confirmed by TEM analysis. The mean size of the core particles varied between 15 and 19 nm along the a,b-direction and 19–27 nm along the c-axis with standard deviations between 8% and 6%, respectively. These size deviations of the active volume (core) in the range of maximum 4–5 nm are sufficiently small to not cover the doping effects to be assessed. For the single particle studies presented in a forthcoming section, we nevertheless considered these deviations and corrected the obtained results for the number of active lanthanide ions per UCNC. The core/shell particles always show a shell thickness twice the core dimension in *a*,*b*- and *c*-direction with maximum variations of 20%. TEM images of core and core/shell particles with 60% Yb^{3+} and 2% Er^{3+} are exemplarily shown in Fig. 1. The size histograms as well as the TEM images and size histograms of UCNC with other dopant concentrations are provided in Figs. S1–S7 in the ESM. The hexagonal crystal phases of the UCNC were confirmed by XRD (Figs. S8–S11 in the ESM).

3.2 Upconversion luminescence features of highly doped UCNC

3.2.1 *Yb^{3+} concentration series*

First, the *P*-dependent Φ_{UC} and UCL decay kinetics of the UCNC of the Yb^{3+} concentration series, i.e., $NaYF_4$:Yb,Er core particles co-doped with 20%, 40%, 60%, 80%, and 98% Yb^{3+} and 2% Er^{3+} were determined. All particles were protected by a $Na(Y,Lu)F_4$ shell containing between 22% Lu^{3+} (in the case of the $NaYF_4$:2%Er, 20%Yb core particles) and 100% Lu^{3+} (in the case of the $NaYbF_4$:2%Er core particles). All measurements were done with powdered samples to circumvent an influence of solvent molecules on the UCL features in this fundamental study [40].

The UCL spectra of these UCNC display the typical green

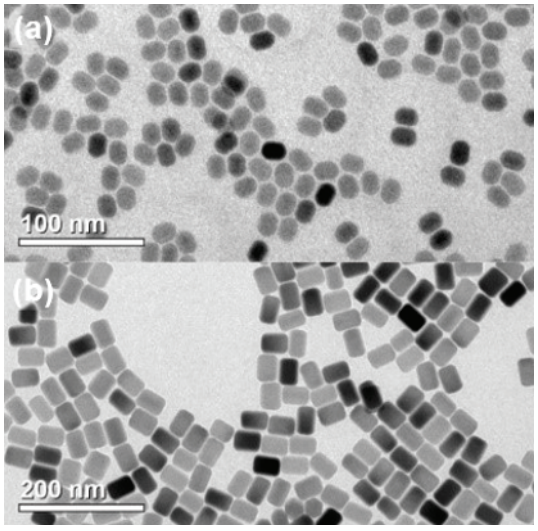

Figure 1 TEM image of β-$NaYF_4$:60%Yb,2%Er core particles (top) and β-$NaYF_4$:60%Yb,2%Er/$NaYF_4$:62%Lu core/shell particles (bottom). The shell increases the particle length (crystallographic c-axis) from 19.4 nm ± 4.1% to 42 nm ± 4.8% and the particle width from 14.1 nm ± 6% to 29.9 nm ± 7.8%. An increase by a factor of two is expected, as the core particles and the shell precursor were combined in a molar ratio of 1 to 7. Note the different scale bars in the TEM images. TEM images and size histograms of all particles are shown in the ESM.

(510–570 nm) and red Er^{3+} emission bands (635–658 nm) as well as the less pronounced Er^{3+} emission bands in the NIR (783–860 nm) and ultraviolet (394–430 nm). The UCL spectra are shown in Figs. S12 and S13 in the ESM. The relative spectral contribution of the different Er^{3+} emission bands to overall UCL depend on P as reported before. The P dependences of the Φ_{UC} of these particle powders are compared in Fig. 2(a)). The $NaYF_4$:20%Yb,2%Er/$NaYF_4$:22% Lu core/shell particles display a maximum Φ_{UC} value of 9.5%, which is practically identical with that of the microcrystalline upconversion phosphor $NaYF_4$:20%Yb,2%Er. This confirms our earlier results obtained for $NaYF_4$:18%Yb,2%Er/$NaYF_4$ core/shell particles lacking Lu^{3+} in the shell [41]. It also shows that Lu^{3+} doping of the shell has no negative effect on Φ_{UC}. Remarkably, the Φ_{UC} values decrease only slightly when the Yb^{3+} concentration in the core particle is increased from 20% to 98%. For all samples, the intensity ratio of the red emission to the green emission, i.e., the red-to green ratio, increases with increasing P (Fig. 2(b); the corresponding UCL spectra are shown in Fig. S12 in the ESM). The crossing points, that are, the P values for which the intensity of the green Er^{3+} emission band equals the intensity of the red Er^{3+} emission band, shift systematically to lower P values with increasing Yb^{3+} concentration. This is ascribed to an enhanced population of high Er^{3+} energy levels involving population processes of higher photonic order. Please note that for the measurements of

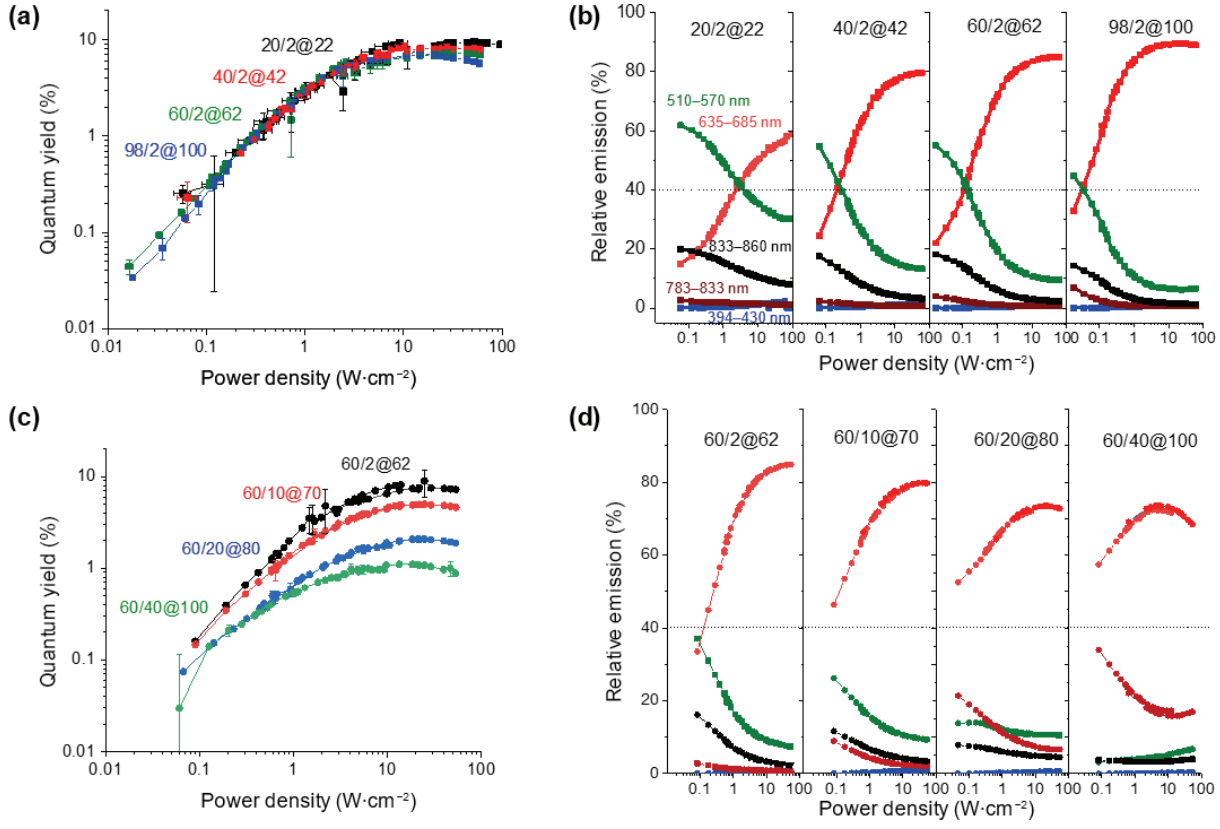

Figure 2 (a) Upconversion quantum yield Φ_{UC} of β-$NaYF_4$:Yb,Er/$NaYF_4$:Lu core/shell particles as a function of excitation power density (P). Φ_{UC} of the particles doped with 2% Er^{3+} decreases only slightly when the Yb^{3+} concentration is increased from 20% (black) to 40% (red), 60% (green), and 98% (blue), respectively. Core/shell particles doped with 20% Yb^{3+} display a record maximum Φ_{UC} of 9.5% close to the Φ_{UC} of high-quality microcrystalline upconversion phosphor powder [41]. (b) Relative ratios of the differently colored UC emission bands of core/shell particles doped with 2% Er^{3+} and different Yb^{3+} concentrations of 20%, 40 %, 60 %, and 98 % as a function of P. Each diagram shows the relative contributions of the red emission (635–658 nm), green emission (510–570 nm), NIR emission at 810 nm (783–833 nm – brown) and 845 nm (833–860 nm), and blue emission (394–430 nm) to the total UC emission of the Er^{3+} ions. The crossing point of the red and green emission, i.e., the P value where the red and the green emission match in intensity, shifts systematically to lower P values with increasing Yb^{3+} dopant concentration. (c) Φ_{UC} of β-$NaYF_4$:Yb,Er/$NaYF_4$:Lu core/shell particles doped with different Er^{3+} concentrations as a function of P. Φ_{UC} of particles doped with 60% Yb^{3+} decreases by approximately one order of magnitude when the Er^{3+} concentration is increased from 2% (black) to 40% (red). (d) Relative ratios of the differently colored UC emission bands of core/shell particles doped with 60% Yb^{3+} and Er^{3+} concentrations of 2%, 10%, 20%, and 40% as a function of P. Each diagram shows the relative contributions of the red emission (635–658 nm), green emission (510–570 nm), NIR emission at 810 nm (783–833 nm – brown) and 845 nm (833–860 nm), and the blue emission (394–430 nm) to the total UC emission of the Er^{3+} ions.

powdered samples *P* has to be kept lower than for measurements of dispersed UCNC to prevent the decomposition of the organic surface ligands [40].

These experiments clearly demonstrate that the Yb^{3+} concentration and, hence, the absorption cross section of the UCNC can be strongly increased without sacrificing a high Φ_{UC}. Similar trends have been also reported by other research groups [18, 22], but were not quantified in terms of absolutely measured Φ_{UC} data. This result is also reflected by the decay kinetics and luminescence lifetimes of the Yb^{3+} emission displayed in Fig. 3 and Fig. S14(a) in the ESM), which generally show long Yb^{3+} lifetimes without a systematic dependence on Yb^{3+} concentration. This indicates that higher Yb^{3+} concentrations neither increase the total number of quenching sites, for instance at the core/shell interface, nor the probability that the excitation energy reaches additional quenching sites due to faster energy migration. The latter was also minimized by our elaborate UCNC synthesis. The long Yb^{3+} lifetimes not only underline a low defect density at the core/shell interface but also tight surface passivation shells which are sufficiently thick to block energy transfer to the particle surface. In addition, this finding indicates that the mixing of highly Yb^{3+} doped core material into the surface shells is sufficiently low during shell growth for our syntheses.

3.2.2 Er^{3+} concentration series

Based on the results obtained with the Yb^{3+} concentration series, subsequently, we prepared $NaYF_4$:Yb,Er core particles doped with 60% of Yb^{3+} and Er^{3+} concentrations varying between 2% up to 40%. These core particles were then protected with a $Na(Y,Lu)F_4$ shell containing between 62% Lu^{3+} (in case of the $NaYF_4$:2% Er, 60% Yb core particle) and 100% Lu^{3+} (in case of the $NaYbF_4$: 40% Er core particles). The results of the spectroscopic studies of the Er^{3+} concentration series are shown in Figs. 2 and 3 and Fig. S13 in the ESM). As follows from the UCL spectra provided in Fig. S13 in the ESM, an increase in Er^{3+} concentration enhances the red Er^{3+} emission and the NIR Er^{3+} emission at 810 nm. As displayed in Fig. 2(c)), with increasing Er^{3+} concentration, Φ_{UC} decreases. Overall, Φ_{UC} is reduced by about a factor of seven when the Er^{3+} concentration is increased from 2% to 40%. The lower Φ_{UC} values obtained for the Er^{3+} concentration series are expected, since high Er^{3+} concentrations are known to favor cross relaxation of the Er^{3+} ions leading to UCL quenching. The strong interactions between neighboring Er^{3+} ions at high Er^{3+} concentrations are reflected by a reduced intensity of the green Er^{3+} emission and a relatively high intensity of the red Er^{3+} emission as well as by the relatively strong NIR emission at 810 nm as highlighted in Fig. 2(d)) and in Fig. S13 in the ESM, summarizing the corresponding emission spectra). The latter is known to result from increased Er^{3+}-Er^{3+} ETU processes involving the first excited Er^{3+} state [15, 54].

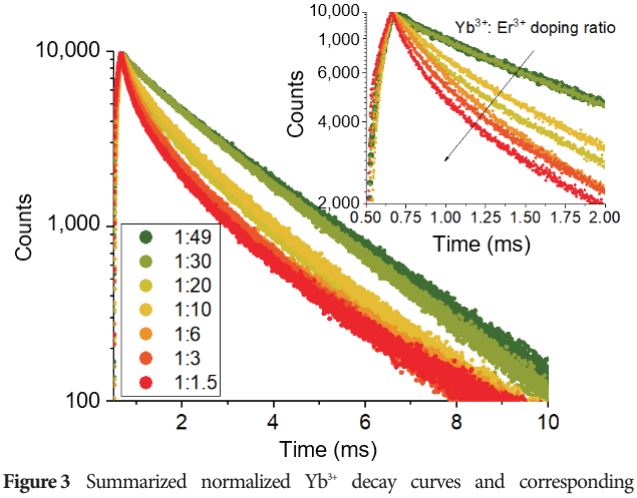

Figure 3 Summarized normalized Yb^{3+} decay curves and corresponding doping ratio normalized to the Er^{3+} concentration. The reduced Yb^{3+} decay time indicates higher energy transfer rates for Er^{3+} concentrations approaching the Yb^{3+} doping concentrations. The Yb^{3+} luminescence was excited at 978 nm and recorded at 1000 nm.

Interestingly, the lifetime of the Yb^{3+} emission, that provides a hint and measure for quenching processes, also remains long for the Er^{3+} concentration series. This is highlighted in Fig. 3, summarizing the luminescence decay curves of the UCNC varying in Yb^{3+}-to-Er^{3+} doping ratios (normalized to the Er^{3+} concentration) on two slightly different time scales used to better visualize the trends. The corresponding Yb^{3+} decay kinetics of the Yb^{3+} and Er^{3+} concentration series are given in Figs. S14(a) and S14(b) in the ESM. The generally long luminescence lifetime of the Yb^{3+} emission indicates an excellent shielding of the particle core in all cases while its diminution, i.e., the appearance of short decay components observed for increasing amounts of Er^{3+} is ascribed to higher energy transfer rates caused by reduced Er-Yb distances.

3.2.3 UCL measurements at very high *P*

To exemplarily assess the influence of high *P* (> 1 MW/cm²) on the UCL characteristics of highly doped UCNC we performed first measurements with selected UCNC deposited on a substrate and a home-built single particle setup previously reported [49]. The goal was here to estimate the performance of our differently doped UCNC under conditions of very high *P* often utilized in microscopic studies [24]. A comparison of the UCL brightness of the differently doped UCNC samples, given as a measured signal size in counts obtained for otherwise identical measurement parameters, is presented in Fig. 4. These measurements utilizing *P* of up to 2 MW/cm² demonstrate that under high-power excitation conditions, the highest emission intensities result for the samples with Yb^{3+}/Er^{3+} doping concentrations of 60%/10% and 60%/20%. Apparently, for high power applications, the Er^{3+} concentration quenching can be compensated by high excitation photon fluxes, which has been earlier explained by a desaturation of Yb^{3+} ions [27]. This confirms the observations of other research groups on highly doped UCNC and their good performance under microscopic, i.e., high-power excitation conditions [29, 38].

4 Conclusion and outlook

In summary, we systematically explored and quantified the influence of high Yb^{3+} and Er^{3+} doping concentrations on the efficiency of the upconversion luminescence (UCL) of core/shell upconversion nanocrystals (UCNC) with core sizes of 20–25 nm. To assess solely the influence of high sensitizer and activator concentrations and to determine compositions and doping ratios optimum for a high UCL quantum yield (Φ_{UC}) and a high particle brightness, two sets of core/shell particles, an Yb^{3+} and an Er^{3+} concentration series were prepared, thereby taking measures to minimize all other possible UCL quenching pathways. This included the use of an elaborate water-free synthetic route previously shown to yield high quality UCNC with record Φ_{UC} and surface shielding with a thick $Na(Y,Lu)F_4$ shell. In addition, only solid UCNC were studied. The particle cores of the Yb^{3+} concentration series were doped with 2% of Er^{3+} and 20%, 40%, 60% 80%, and 98% of Yb^{3+} and those of the Er^{3+} concentration series with 60% of Yb^{3+} and 2%, 10%, 20%, and 40% of Er^{3+}. Carefully choosing water-free reactants and optimum synthetic conditions gave $NaYF_4$:Yb,Er UCNC with a high Φ_{UC} and very long lifetimes of the Yb^{3+} emission. At low Er^{3+} concentration, the Φ_{UC} values approached Φ_{UC} of a high quality microcrystalline upconversion phosphor and remained high even

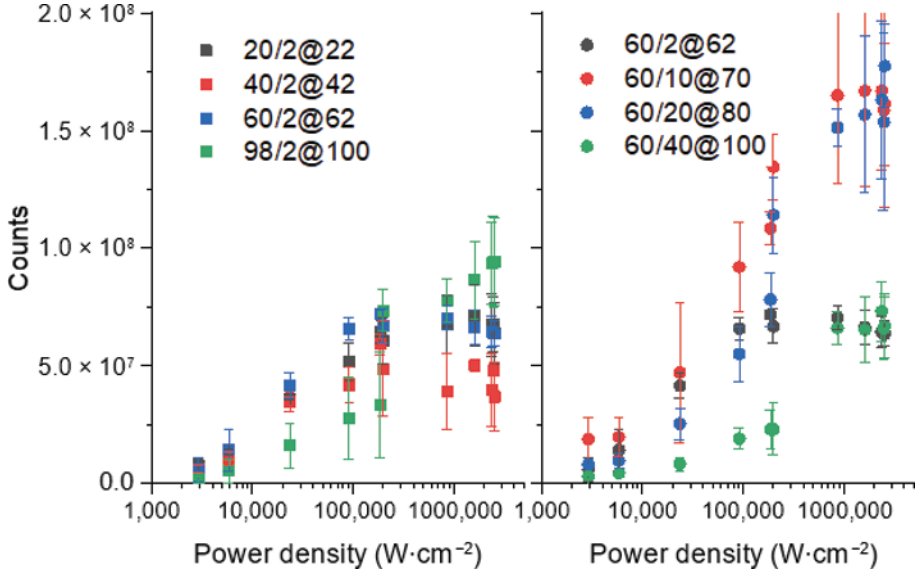

Figure 4 Luminescence emission intensities of single β-$NaYF_4$:Yb,Er/$NaYF_4$ core/shell particles at high excitation power densities (> 1 MW/cm²). (a) UCNC doped with 2% Er^{3+} and 20% (black), 40% (red), 60% (blue), and 98% (green) of Yb^{3+}, respectively. (b) UCNC doped with 60% Yb^{3+} and 2% (black), 10% (red), 20% (blue), and 40% (green) of Er^{3+}, respectively.

for very high Yb^{3+} concentrations. Increasing the Er^{3+} concentration, however, reduced Φ_{UC} and enhanced the relative spectral contribution of the red and NIR Er^{3+}emission bands to overall UCL as previously observed for other "quenched" UCNC. Single particle studies done to realize high excitation power densities (P) of up to 2 MW/cm² revealed that Er^{3+} concentration quenching can be compensated by high excitation photon fluxes. In this case, the highest emission intensities were obtained for UCNC samples with 60/10 and 60/20 Yb^{3+}/Er^{3+} doping concentrations. Hence, for high power applications, highly doped UCNC are a better choice than UCNC containing the conventionally used Yb^{3+} and Er^{3+} concentrations of 20% and 2%.

Our results also confirm the important influence of the synthesis on the quality of the resulting UCNC and underline its mandatory control for achieving high Φ_{UC} and a high particle brightness. For all applications utilizing high P, however, UCL quenching by defect sites at the particle surface or within the particle can be most likely compensated by P, thereby reducing the requirements on UCNC quality and UCNC design. Under these conditions, a high absorption cross section as provided by heavily doping with Yb^{3+} becomes increasingly beneficial. Overall, the results of our quantitative concentration studies will pave the road to the design of more fundamental photophysical studies of UCNC and to UCNC of increased brightness for different P regimes and applications in the life and material sciences.

Acknowledgements

We thank the German Science Foundation DFG (grants RE 1203/18-1 and HA 1649/7-1) and the EU (COST 1403) for financial support.

Funding note: Funding note Open Access funding enabled and organized by Projekt DEAL.

Electronic Supplementary Material: Supplementary material is available in the online version of this article at https://doi.org/10.1007/s12274-022-4570-5.

References

[1] Haase, M.; Schäfer, H. Upconverting nanoparticles. *Angew. Chem. , Int. Ed.* **2011**, *50*, 5808–5829.

[2] Chen, G. Y.; Ågren, H.; Ohulchanskyy, T. Y.; Prasad, P. N. Light upconverting core-shell nanostructures: Nanophotonic control for emerging applications. *Chem. Soc. Rev.* **2015**, *44*, 1680–1713.

[3] Resch-Genger, U.; Gorris, H. H. Perspectives and challenges of photon-upconversion nanoparticles - Part I: Routes to brighter particles and quantitative spectroscopic studies. *Analy. Bioanal. Chem.* **2017**, *409*, 5855–5874.

[4] Himmelstoss, S. F.; Hirsch, T. A critical comparison of lanthanide based upconversion nanoparticles to fluorescent proteins, semiconductor quantum dots, and carbon dots for use in optical sensing and imaging. *Methods Appl. Fluoresc.* **2019**, *7*, 022002.

[5] Wilhelm, S. Perspectives for upconverting nanoparticles. *ACS Nano* **2017**, *11*, 10644–10653.

[6] Zhou, J. J.; Leaño, J. L. Jr; Liu, Z. Y.; Jin, D. Y.; Wong, K. L.; Liu, R. S.; Bünzli, J. C. G. Impact of lanthanide nanomaterials on photonic devices and smart applications. *Small* **2018**, *14*, 1801882.

[7] Qin, X.; Xu, J. H.; Wu, Y. M.; Liu, X. G. Energy-transfer editing in lanthanide-activated upconversion nanocrystals: A toolbox for emerging applications. *ACS Cent. Sci.* **2019**, *5*, 29–42.

[8] Chen, S.; Weitemier, A. Z.; Zeng, X.; He, L. M.; Wang, X. Y.; Tao, Y. Q.; Huang, A. J. Y.; Hashimotodani, Y.; Kano, M.; Iwasaki, H. et al. Near-infrared deep brain stimulation via upconversion nanoparticle-mediated optogenetics. *Science* **2018**, *359*, 679–684.

[9] Shikha, S.; Salafi, T.; Cheng, J. T.; Zhang, Y. Versatile design and synthesis of nano-barcodes. *Chem. Soc. Rev.* **2017**, *46*, 7054–7093.

[10] Goldschmidt, J. C.; Fischer, S. Upconversion for photovoltaics - a review of materials, devices and concepts for performance enhancement. *Adv. Opt. Mater.* **2015**, *3*, 510–535.

[11] Auzel, F. Upconversion and anti-stokes processes with f and d ions in solids. *Chem. Rev.* **2004**, *104*, 139–174.
[12] Tan, M. L.; Monks, M. J.; Huang, D. X.; Meng, Y. J.; Chen, X. W.; Zhou, Y.; Lim, S. F.; Würth, C.; Resch-Genger, U.; Chen, G. Y. Efficient sub-15 nm cubic-phase core/shell upconversion nanoparticles as reporters for ensemble and single particle studies. *Nanoscale* **2020**, *12*, 10592–10599.
[13] Gargas, D. J.; Chan, E. M.; Ostrowski, A. D.; Aloni, S.; Altoe, M. V. P.; Barnard, E. S.; Sanii, B.; Urban, J. J.; Milliron, D. J.; Cohen, B. E. et al. Engineering bright sub-10-nm upconverting nanocrystals for single-molecule imaging. *Nat. Nanotechnol.* **2014**, *9*, 300–305.
[14] Würth, C.; manley, P.; voigt, R.; ahiboz, D.; becker, C.; resch-genger, U. Metasurface enhanced sensitized photon upconversion: Toward highly efficient low power upconversion applications and nanoscale e-field sensors. *Nano Lett.* **2020**, *20*, 6682–6689.
[15] Würth, C.; Kaiser, M.; Wilhelm, S.; Grauel, B.; Hirsch, T.; Resch-Genger, U. Excitation power dependent population pathways and absolute quantum yields of upconversion nanoparticles in different solvents. *Nanoscale* **2017**, *9*, 4283–4294.
[16] Blasse, G. Luminescence of inorganic solids: From isolated centres to concentrated systems. *Prog. Solid State Chem.* **1988**, *18*, 79–171.
[17] Muhr, V.; Wurth, C.; Kraft, M.; Buchner, M.; Baeumner, A. J.; Resch-Genger, U.; Hirsch, T. Particle-size-dependent forster resonance energy transfer from upconversion nanoparticles to organic dyes. *Anal. Chem.* **2017**, *89*, 4868–4874.
[18] Wang, Z. J.; Meijerink, A. Concentration quenching in upconversion nanocrystals. *J. Phys. Chem. C* **2018**, *122*, 26298–26306.
[19] Chen, G. Y.; Ohulchanskyy, T. Y.; Kumar, R.; Ågren, H.; Prasad, P. N. Ultrasmall monodisperse $NaYF_4$: Yb^{3+}/Tm^{3+} nanocrystals with enhanced near-infrared to near-infrared upconversion photoluminescence. *ACS Nano* **2010**, *4*, 3163–3168.
[20] Gao, D. L.; Zhang, X. Y.; Chong, B.; Xiao, G. Q.; Tian, D. P. Simultaneous spectra and dynamics processes tuning of a single upconversion microtube through Yb^{3+} doping concentration and excitation power. *Phys. Chem. Chem. Phys.* **2017**, *19*, 4288–4296.
[21] Podhorodecki, A.; Krajnik, B.; Golacki, L. W.; Kostiv, U.; Pawlik, G.; Kaczmarek, M.; Horak, D. Percolation limited emission intensity from upconverting $NaYF_4$: Yb^{3+}, Er^{3+} nanocrystals-a single nanocrystal optical study. *Nanoscale* **2018**, *10*, 21186–21196.
[22] Shen, B.; Cheng, S. M.; Gu, Y. Y.; Ni, D. R.; Gao, Y. L.; Su, Q. Q.; Feng, W.; Li, F. Y. Revisiting the optimized doping ratio in core/shell nanostructured upconversion particles. *Nanoscale* **2017**, *9*, 1964–1971.
[23] Ma, C. S. ; Xu, X. X. ; Wang, F. ; Zhou, Z. G. ; Liu, D. M. ; Zhao, J. B. ; Guan, M. ; Lang, C. I. ; Jin, D. Y. Optimal sensitizer concentration in single upconversion nanocrystals. *Nano Lett.* **2017**, *17*, 2858–2864.
[24] Liu, Q.; Zhang, Y. X.; Peng, C. S.; Yang, T. S.; Joubert, L. M.; Chu, S. Single upconversion nanoparticle imaging at sub-10 $W \cdot cm^{-2}$ irradiance. *Nat. Photonics* **2018**, *12*, 548–553.
[25] Chan, E. M.; Levy, E. S.; Cohen, B. E. Rationally designed energy transfer in upconverting nanoparticles. *Adv. Mater.* **2015**, *27*, 5753–5761.
[26] Zhao, J. B.; Jin, D. Y.; Schartner, E. P.; Lu, Y. Q.; Liu, Y. J.; Zvyagin, A. V.; Zhang, L. X.; Dawes, J. M.; Xi, P.; Piper, J. A. et al. Single-nanocrystal sensitivity achieved by enhanced upconversion luminescence. *Nat. Nanotechnol.* **2013**, *8*, 729–734.
[27] Tian, B. N.; Fernandez-Bravo, A.; Najafiaghdam, H.; Torquato, N. A.; Altoe, M. V. P.; Teitelboim, A.; Tajon, C. A.; Tian, Y.; Borys, N. J.; Barnard, E. S. et al. Low irradiance multiphoton imaging with alloyed lanthanide nanocrystals. *Nat. Commun.* **2018**, *9*, 3082.
[28] Teitelboim, A.; Tian, B. N.; Garfield, D. J.; Fernandez-Bravo, A.; Gotlin, A. C.; Schuck, P. J.; Cohen, B. E.; Chan, E. M. Energy transfer networks within upconverting nanoparticles are complex systems with collective, robust, and history-dependent dynamics. *J. Phys. Chem. C* **2019**, *123*, 2678–2689.
[29] Chen, B.; Wang, F. Combating concentration quenching in upconversion nanoparticles. *Acc. Chem. Res.* **2020**, *53*, 358–367.
[30] Chen, B.; Wang, F. Recent advances in the synthesis and application of Yb-based fluoride upconversion nanoparticles. *Inorg. Chem. Front.* **2020**, *7*, 1067–1081.
[31] Zhou, B.; Tang, B.; Zhang, C.; Qin, C. Y.; Gu, Z. J.; Ma, Y.; Zhai, T. Y.; Yao, J. N. Enhancing multiphoton upconversion through interfacial energy transfer in multilayered nanoparticles. *Nat. Commun.* **2020**, *11*, 1174.
[32] Sun, L. Y.; Gao, R. Y.; Pan, T. T.; Ai, X. C.; Fu, L. M.; Zhang, J. P. Concentration-regulated photon upconversion and quenching in $NaYF_4$: Yb^{3+}, Er^{3+} nanocrystals: Nonexponentiality revisited. *Nanoscale* **2019**, *11*, 18150–18158.
[33] Rabouw, F. T.; Prins, P. T.; Villanueva-Delgado, P.; Castelijns, M.; Geitenbeek, R. G.; Meijerink, A. Quenching pathways in $NaYF_4$: Er^{3+}, Yb^{3+} upconversion nanocrystals. *ACS Nano* **2018**, *12*, 4812–4823.
[34] Hossan, Y.; Hor, A.; Luu, Q.; Smith, S. J.; May, P. S.; Berry, M. T. Explaining the nanoscale effect in the upconversion dynamics of β-$NaYF_4$: Yb^{3+}, Er^{3+} core and core-shell nanocrystals. *J. Phys. Chem. C* **2017**, *121*, 16592–16606.
[35] Kraft, M.; Würth, C.; Muhr, V.; Hirsch, T.; Resch-Genger, U. Particle-size-dependent upconversion luminescence of $NaYF_4$: Yb, Er nanoparticles in organic solvents and water at different excitation power densities. *Nano Res.* **2018**, *11*, 6360–6374.
[36] Wei, W.; Zhang, Y.; Chen, R.; Goggi, J.; Ren, N.; Huang, L.; Bhakoo, K. K.; Sun, H. D.; Tan, T. T. Y. Cross relaxation induced pure red upconversion in activator- and sensitizer-rich lanthanide nanoparticles. *Chem. Mater.* **2014**, *26*, 5183–5186.
[37] Lee, C.; Park, H.; Kim, W.; Park, S. Origin of strong red emission in Er^{3+}-based upconversion materials: Role of intermediate states and cross relaxation. *Phys. Chem. Chem. Phys.* **2019**, *21*, 24026–24033.
[38] Wen, S. H.; Zhou, J. J.; Zheng, K. Z.; Bednarkiewicz, A.; Liu, X. G.; Jin, D. Y. Advances in highly doped upconversion nanoparticles. *Nat. Commun.* **2018**, *9*, 2415.
[39] Zheng, X.; Shikha, S.; Zhang, Y. Elimination of concentration dependent luminescence quenching in surface protected upconversion nanoparticles. *Nanoscale* **2018**, *10*, 16447–16454.
[40] Kaiser, M.; Würth, C.; Kraft, M.; Hyppänen, I.; Soukka, T.; Resch-Genger, U. Power-dependent upconversion quantum yield of $NaYF_4$: Yb^{3+}, Er^{3+} nano- and micrometer-sized particles - measurements and simulations. *Nanoscale* **2017**, *9*, 10051–10058.
[41] Homann, C.; Krukewitt, L.; Frenzel, F.; Grauel, B.; Würth, C.; Resch-Genger, U.; Haase, M. $NaYF_4$: Yb, Er/$NaYF_4$ core/shell nanocrystals with high upconversion luminescence quantum Yield. *Angew. Chem., Int. Ed.* **2018**, *57*, 8765–8769.
[42] Hudry, D.; Busko, D.; Popescu, R.; Gerthsen, D.; Abeykoon, A. M. M.; Kübel, C.; Bergfeldt, T.; Richards, B. S. Direct evidence of significant cation intermixing in upconverting core@shell nanocrystals: Toward a new crystallochemical model. *Chem. Mater.* **2017**, *29*, 9238–9246.
[43] Mondini, S.; Ferretti, A. M.; Puglisi, A.; Ponti, A. PEBBLES and PEBBLEJUGGLER: Software for accurate, unbiased, and fast measurement and analysis of nanoparticle morphology from transmission electron microscopy (TEM) micrographs. *Nanoscale* **2012**, *4*, 5356–5372.
[44] Rodríguez-Carvajal, J. An introduction to the program FullProf. Saclay: Laboratoire Léon Brillouin (CEA-CNRS), 2001.
[45] Cui, X.; Feng, Z.; Jin, Y.; Cao, Y.; Deng, D.; Chu, H.; Cao, S.; Dong, C.; Zhang, J. AutoFP: A GUI for highly automated Rietveld refinement using an expert system algorithm based on *FullProf*. *J. Appl. Cryst.* **2015**, *48*, 1581–1586.
[46] Andresen, E.; Wurth, C.; Prinz, C.; Michaelis, M.; Resch-Genger, U. Time-resolved luminescence spectroscopy for monitoring the stability and dissolution behaviour of upconverting nanocrystals with different surface coatings. *Nanoscale* **2020**, *12*, 12589–12601.
[47] Saleh, M. I.; Rühle, B.; Wang, S.; Radnik, J.; You, Y.; Resch-Genger, U. Assessing the protective effects of different surface coatings on $NaYF_4$: Yb^{3+}, Er^{3+} upconverting nanoparticles in buffer and DMEM. *Sci. Rep.* **2020**, *10*, 19318.
[48] Meijer, M. S.; Rojas-Gutierrez, P. A.; Busko, D.; Howard, I. A.; Frenze, F.; Würth, C.; Resch-Genger, U.; Richards, B. S.; Turshatov, A.; Capobianco, J. A. et al. Absolute upconversion quantum yields of blue-emitting $LiYF_4$: Yb^{3+}, Tm^{3+} upconverting nanoparticles. *Phys. Chem. Chem. Phys.* **2018**, *20*, 22556–22562.
[49] Frenzel, F.; Würth, C.; Dukhno, O.; Przybilla, F.; Wiesholler, L. M.;

Muhr, V.; Hirsch, T.; Mély, Y.; Resch-Genger, U. Multiband emission from single β-$NaYF_4$(Yb, Er) nanoparticles at high excitation power densities and comparison to ensemble studies. *Nano Res.* **2021**, *14*, 4107–4115.

[50] Johnson, N. J. J.; Korinek, A.; Dong, C. H.; Van Veggel, F. C. J. M. Self-focusing by ostwald ripening: A strategy for layer-by-layer epitaxial growth on upconverting nanocrystals. *J. Am. Chem. Soc.* **2012**, *134*, 11068–11071.

[51] Talapin, D. V.; Rogach, A. L.; Haase, M.; Weller, H. Evolution of an ensemble of nanoparticles in a colloidal solution: Theoretical study. *J. Phys. Chem. B* **2001**, *105*, 12278–12285.

[52] Voss, B.; Haase, M. Intrinsic focusing of the particle size distribution in colloids containing nanocrystals of two different crystal phases. *ACS Nano* **2013**, *7*, 11242–11254.

[53] Würth, C.; Fischer, S.; Grauel, B.; Alivisatos, A. P.; Resch-Genger, U. Quantum yields, surface quenching, and passivation efficiency for ultrasmall core/shell upconverting nanoparticles. *J. Am. Chem. Soc.* **2018**, *140*, 4922–4928.

[54] Pollnan, M.; Jackson, S. D. Erbium 3-μm fiber lasers. *IEEE J. Sel. Top. Quantum Electron.* **2001**, *7*, 30–40.